

Pair and many-body interactions between ligated Au nanoparticles

Cite as: J. Chem. Phys. **150**, 044904 (2019); <https://doi.org/10.1063/1.5064545>

Submitted: 05 October 2018 . Accepted: 07 January 2019 . Published Online: 28 January 2019

Christopher Liepold,  Alex Smith,  Binhua Lin, Juan de Pablo, and  Stuart A. Rice



View Online



Export Citation



CrossMark

ARTICLES YOU MAY BE INTERESTED IN

[Understanding interactions between capped nanocrystals: Three-body and chain packing effects](#)

The Journal of Chemical Physics **131**, 124705 (2009); <https://doi.org/10.1063/1.3227043>

[Molecular interaction between asymmetric ligand-capped gold nanocrystals](#)

The Journal of Chemical Physics **150**, 034702 (2019); <https://doi.org/10.1063/1.5065476>

[Explicit all-atom modeling of realistically sized ligand-capped nanocrystals](#)

The Journal of Chemical Physics **136**, 114702 (2012); <https://doi.org/10.1063/1.3689973>



Your Qubits. Measured.

Meet the next generation of quantum analyzers

- Readout for up to 64 qubits
- Operation at up to 8.5 GHz, mixer-calibration-free
- Signal optimization with minimal latency

[Find out more](#)



Pair and many-body interactions between ligated Au nanoparticles

Cite as: *J. Chem. Phys.* **150**, 044904 (2019); doi: [10.1063/1.5064545](https://doi.org/10.1063/1.5064545)

Submitted: 5 October 2018 • Accepted: 7 January 2019 •

Published Online: 28 January 2019



View Online



Export Citation



CrossMark

Christopher Liepold,¹ Alex Smith,¹  Binhua Lin,^{1,2}  Juan de Pablo,³ and Stuart A. Rice^{1,a)} 

AFFILIATIONS

¹James Franck Institute, University of Chicago, Chicago, Illinois 60637, USA

²Center for Advanced Radiation Sources and University of Chicago, Chicago, Illinois 60637, USA

³Institute for Molecular Engineering, University of Chicago, Chicago, Illinois 60637, USA

^{a)}Author to whom correspondence should be addressed: sarice@uchicago.edu

ABSTRACT

We report the results of molecular dynamics simulations of the properties of a pseudo-atom (united atom) model of dodecane thiol ligated 5-nm diameter gold nanoparticles (AuNPs) in a vacuum as a function of ligand coverage and particle separation in three states of aggregation, namely, the isolated AuNPs, the isolated pair of AuNPs, and a square lattice of four AuNPs. Our calculations show that the ligand density along a radius emanating from the core of an isolated AuNP has the same gross features for all values of the coverage; it oscillates around a constant value up to a distance along the chain corresponding to the position of the fourth pseudo-atom and then smoothly decays to zero, reflecting both the restricted conformations of the chain near the core surface and the larger numbers of conformations available further from the core. Interaction between two AuNPs generates changes in the ligand distributions of each. We examine the structure and general shape of the ligand envelope as a function of the coverage and demonstrate that the equilibrium structure of the envelope and the deformation of that envelope generated by interaction between the NPs are coverage-dependent so that the shape, depth, and position of the minimum of the potential of mean force display a systematic dependence on the ligand coverage. We propose an accurate analytical description of the calculated potential of mean force as a function of a set of parameters that scale linearly with the ligand coverage. Noting that the conformational freedom of the ligands implies that multiparticle induced deviations from additivity of the pair potential of mean force are likely important; we define and calculate a “bond stretching” effective pair potential of mean force for a square lattice of particles that contains, implicitly, both the three- and four-NP contributions. We find that the bond stretching effective pair potential of mean force in this cluster has a different minimum and a different well depth from the isolated pair potential of mean force. Previous work has found that the three-particle contribution to deviation from pair additivity is monotonically repulsive, whereas we find that the combined three- and four-particle contributions have an attractive well, implying that the three- and four-particle contributions are of comparable magnitude but opposite sign, thereby suggesting that even higher order correction terms likely play a significant role in the behavior of dense assemblies of many nanoparticles.

Published under license by AIP Publishing. <https://doi.org/10.1063/1.5064545>

I. INTRODUCTION

Interest in the self-assembly into stable monolayers of nanoparticles with tunable electronic, optical, and magnetic properties has been driven by the opportunities to design devices that are very thin yet remarkably strong.¹⁻⁹ The constituents of such a monolayer are typically Au and semiconductor nanocrystals (cores) that are covered with organic

molecule ligands, hereafter referred to as nanoparticles (NPs). A ligand dressed nanocrystal is a very complicated many body system, so theoretical analyses of its properties, whether isolated or assembled in a monolayer, necessarily utilize simplified models of the ligand structure and the molecular interactions. A substantial number of molecular dynamics simulation studies of the ligand structure of isolated NPs and of the interactions between NPs that utilize these models have

been reported.¹⁰⁻³⁷ The more sophisticated of these investigations involve simulations that use full atom¹⁰⁻¹⁸ and pseudo-atom (united atom) force fields,¹⁹⁻²⁹ amongst which are a few investigations of the importance of the three NP interaction level deviation from additivity of the pair potential of mean force.^{23,24,38-40} The results obtained from these simulations establish that the interaction between the ligands of the dressed nanoparticles, not the core-core interaction, determines the NP monolayer mechanical properties. The interpretations of the results of the simulations derived from the several approaches, taken together, are qualitatively consistent, albeit with some differences that are specific to the model representations of the NP. For the much-studied NP with the Au core, the most important common features of the NP ligand structure and the NP-NP interaction obtained from the calculations can be broadly characterized as follows: First, in a vacuum:

- (1) The distribution of conformations of the ligands that dress an isolated Au core is sensitive to the core size and ligand density but relatively insensitive to the core shape except for small (<3 nm) cores.^{10,18,27,28,36} The angular distribution of ligands bound to a small core is much broader and more nearly uniform than that of ligands bound to a large core due to the lower maximum density of ligand dressing of the facets of a small core.^{17,26,27,34}
- (2) For typical ligands, at the minimum of the NP-NP pair potential of mean force the core-core interaction is negligible relative to the ligand-ligand interaction. The equilibrium separation and the well depth of the NP-NP pair potential of mean force increase with the ligand length and the ligand dressing density.^{24,29,37}
- (3) Because each NP is a complex system with many degrees of freedom, in a many NP assembly there are important deviations from additivity of the pair potential of mean force so that the effective force between a pair of particles is affected by the presence of third, fourth, . . . , proximate particles. The available calculations show that the three-particle correction to additivity of the pair potential of mean force is an everywhere repulsive function of the NP-NP pair separation.^{23,35,36}
- (4) When NPs with small cores are assembled in a two- or three-dimensional crystal, there is a threshold ligand coverage, dependent on the ligand length, below which the Au cores sinter. In a three-dimensional face centered cubic crystal composed of NPs with Au cores of 2.8 nm diameter that are dressed with hexane thiol ligands that threshold is about 50% coverage; when dressed with decanethiol that threshold is about 80% coverage.²³ Second, when the NPs are immersed in solvent:
- (5) The dry (vacuum) and wet (immersed in solvent) NP-NP pair potentials of mean force are very different. When the NP is immersed in a solvent, the ligand conformations depend on the qualitative character of the ligand-solvent interaction.^{13,16,19-21,25,30,31} Using polymer chemistry terminology, a good solvent is one in

which the ligand is soluble and in which it has extended conformations; a bad solvent is one in which the ligand is insoluble and in which it has compact conformations. Consequently, the wet NP pair potential of mean force is, typically, everywhere repulsive when the solvent is good and has a strong minimum when the solvent is bad.^{11,12,14,15,22,32}

A NP monolayer is typically dry, so its mechanical properties should be traceable to characteristic features of the ligand structure and consequent NP interactions in a vacuum. The information available concerning these features has gaps that need to be filled for a better understanding of the source of the strength and other mechanical properties of a dry NP monolayer, specifically how these properties depend on the ligand structure and more information on the role played by the environment of the monolayer. Reports of the role of the environment have, to date, only concerned the case of NPs in a dense liquid solvent. However, the influence of solvent on the NP-NP interaction is perceptible on exposure to a very small amount of solvent. For example, experiments reveal that the exposure of a dry AuNP monolayer to water vapor, and its removal, generates a reversible change of the Young's modulus by almost one order of magnitude.⁴¹ Understanding how the low concentration of water molecules at room temperature ambient vapor pressure can generate a large change in the mechanical properties of a NP monolayer requires a detailed treatment of water-ligand interactions and the consequent ligand conformation changes.

In this paper, we contribute to a better understanding of the relationships between ligand conformation, ligand shell redistribution, and the character of the NP pair potential of mean force in a vacuum. We report the results of simulations of the interaction between model nanoparticles consisting of gold cores ligated with dodecane thiol ($\text{CH}_3(\text{CH}_2)_{11}\text{S}$) chains using a pseudo-atom representation of the ligand chains. In addition to their intrinsic interest, these simulations of the NP-NP pair potential of mean force provide a foundation for studying the importance of many particle contributions to the interaction in an assembly of NPs, a subject we address in Sec. IV.

The results of our simulations add to the description of the dry NP-NP interaction in the following ways:

- (1) Our calculations of the interaction between two NPs with dodecane thiol dressed 5 nm Au cores include a wide range of ligand coverages; they reveal the changes in ligand conformations, the changes in position and depth of the minimum of the pair potential of mean force, and the change in shape of that minimum, as a function of ligand coverage.
- (2) We develop an accurate analytic representation of the pair potential of mean force as a function of NP-NP spacing that is valid over the full range of ligand coverage that permits its calculation for arbitrary ligand coverage.
- (3) We report calculations of the variation in the number density of atoms along the ligand chain as a function of

ligand coverage in an isolated NP, revealing how very restricted intra-molecular atomic motion near the surface yields to much less restricted motion of the ligand chain beyond four atoms from the binding site.

- (4) We show that the general shape of the distribution of ligands around the core is affected by the NP-NP interaction in different ways for different coverages. Our calculations of the number density of atoms along the ligand chain for different ligand coverages as a function of angular difference from the NP-NP centerline reveal the response of the ligand chain distribution to ligand-ligand overlap.
- (5) We provide an estimate of the many NP induced deviation from additivity of the pair potential of mean force that arises from three- and four-particle proximity to a pair of NPs. Our estimate uses a different representation of the non-additivity from commonly reported.⁴⁰ Rather than explicitly calculating the incremental third NP and fourth NP contributions to the effective force between a pair of NPs, we exploit the very limited range of the pair potential of mean force to define an effective pair potential of mean force and its variation with NP-NP separation. Our effective pair potential of mean force contains contributions from proximate third and fourth NPs. It is obtained from calculations of the total interaction free energy of a square configuration of four NPs followed by division by the number of NP-NP nearest neighbors; its separation dependence is determined by varying the side length of the square. The definition clearly includes the contributions to the nearest neighbor interaction from proximate third and fourth NPs, subject to the approximation that the NP-NP interaction along the diagonal of the square is negligibly small. The latter approximation is consistent with the range of the isolated NP-NP pair potential of mean force. The calculated combined three- and four-particle interaction correction to additivity of the pair potential of mean force has a consistent dependence on ligand coverage. Accounting for these interactions generates an effective pair potential of mean force with an equilibrium spacing that increases with increasing ligand coverage but, compared with the corresponding isolated NP-NP pair potentials of mean force, has a smaller well depth when the ligand coverage is large (96%) and a greater well depth when the ligand coverage is small (32%).
- (6) The three- and four-particle interaction corrections to additivity of the pair potential of mean force are of comparable magnitude, which suggests that contributions to the effective pair potential of mean force from proximity to yet more particles, e.g., fifth and sixth neighbors in a two-dimensional array, may be significant.

II. PSEUDO-ATOM MODEL AND CALCULATION DETAILS

As a prelude to the description of our simulation model and details of our calculations, it is worthwhile to collect some general observations. Because a single dressed nanoparticle is

a complex system with many degrees of freedom, a key ingredient in the NP-NP interaction is the response of the ligand conformations to changing particle-particle separation. Calculation of the change in free energy that follows execution of a change in that separation involves averages over all conformations of the dressing ligands and, when relevant, NP rotations. Nanoparticles in a liquid suspension are free to rotate, whereas NPs in a dry film are constrained to not rotate by virtue of the ligand-ligand interactions. If the ligands bound to the nanoparticle are mobile on the core surface, the free energy change that accompanies changing the separation of the NPs also involves averaging over the responsive alteration in the surface distribution of ligands. And, as already mentioned in the Introduction, since the presence of a proximate third NP will, in principle, alter all of the ligand conformations, the total free energy of interaction of three NPs will not be accurately represented as a sum of the free energies of interaction of isolated NP pairs, i.e., the total free energy of interaction of an assembly of NPs is then not pair additive. Given the complexity of conformations associated with the ligands, it is reasonable to expect further deviations from pair additivity when the free energies of four, five, . . . , NP configurations are evaluated.

The shape of the core of an Au nanoparticle depends on the number of atoms in that core. In general, we can think of the core as a truncated lattice with a particular shape. For small cores ($D < 5$ nm), this truncated lattice is icosahedral, for moderate size cores ($5 \text{ nm} < D < 10$ nm) it is dodecahedral, and for larger cores it takes shapes associated with various truncated fcc lattices.^{42,43} However, explicit treatments of the equilibrium structure of the gold core have shown that under the temperatures and stresses required for the formation of these particles, the edges of the crystal will soften and become somewhat rounded.⁴⁴ Consequently, we expect the 5 nm diameter cores in our model to form either an icosahedron or a dodecahedron with smoothed edges. Even within monodisperse samples, populations of both icosahedron and dodecahedron shapes are found to coexist.⁴³ Because of this coexistence, the smoothing of the particle edges, and the relatively small size of the lattice facets, all of our calculations use the approximation that the gold cores are spherical. Specifically, in our model the Au cores are taken to be uniform spheres constructed from identical particles that interact with a Lennard-Jones potential. An effective potential of this form has been calculated by Everaers and Ejtehadi,⁴⁵ which we use for the core-pseudo-atom interactions in our system; the parameters and functional form are tabulated in [Tables I and II](#) of the [Appendix](#).

Our simplified model of the ligand molecule represents it as a thirteen-particle chain with three types of pseudo-atoms for the CH_2 , CH_3 , and S moieties. All pseudo-atoms except those that are nearest neighbors along a chain interact through direct Lennard-Jones style potentials, while nearest neighbors interact with a harmonic bonding potential. The cis-trans structure of the chain and the barrier to internal rotation are characterized by describing the bending of triplets on the chain with a harmonic angular potential and the twisting motion of quadruplets along the chain with a torsion

potential. The parameters and functional forms of each of these potentials are provided in Tables I and II. The specific forms we have chosen for the potentials are borrowed from Paul *et al.*,⁴⁶ who found that they describe well the experimental equation of state behavior and the local mobility of chains in a melt. Our model of the ligand molecule also retains the qualitative character of the conformations obtained from molecular mechanics (MM3) calculations more closely than do the conformations supported by the Optimal Potential for Liquid Simulations-United Atom (OPLS-UA) and Optimal Potential for Liquid Simulations-All Atom (OPLS-AA) force fields.²⁷

There is some evidence that when dressed nanoparticles such as we consider are in solution the ligands are mobile along the gold surface, whereas they are immobile in a vacuum.⁴⁷ Since we are interested in the mechanical properties of a dry NP monolayer, we focus attention on the NP-NP interaction in a vacuum, for which case we have fixed the ligand binding sites, equidistant from one another, on the Au core. This constraint imposes an inhomogeneity on the ligand distribution and a loss of rotational symmetry of the NP. If we suppress the rotational motion of the NP, we generate a range of possible interactions between pairs of NPs. For example, if the orientation between the two NPs is such that a ligand is bound very near the center-to-center axis we expect that at small core-core separations the ligand will tilt away from the axis. Conversely, if there are bare portions of the cores along the center-to-center axis, at small separation the total interaction is dominated by the core-core interaction. Simply put, the repulsive interaction at small particle-particle separation will be strongly dependent on the relative orientation of the distributions of ligands that cap those particles. We then expect that interaction between NPs with only a few ligands will have much more variation with orientation than will that between particles that are heavily coated with ligands. We have studied this variation by carrying out simulations with different orientations of the attached ligands and simulations with different coverages of ligands. For dodecane thiol ligands on a flat substrate, the expected maximum coverage provides each ligand with an area per molecule $A = 21.3 \text{ \AA}^2$, corresponding to a surface number density $\rho = 4.7 \text{ nm}^{-2}$, which we define to be $C = 1$.⁴⁸⁻⁵⁰ In our calculations, the coverage of the NP varied from the low value $C = 0.11$ ($\rho = 0.5 \text{ nm}^{-2}$, $A = 200 \text{ \AA}^2$), corresponding to a nearly bare Au core, up to $C = 0.96$ ($\rho = 4.5 \text{ nm}^{-2}$, $A = 22.2 \text{ \AA}^2$), corresponding to the highest coverage experimentally available.

To calculate the free energy of a pair of NPs as a function of separation we proceed as follows: for any selected fixed NP-NP separation we first carry out simulations with fixed NP-NP orientation. In these simulations, the core and sulfur pseudo-atoms interact with every other particle in the system but remain stationary, while the attached ligands come to conformational equilibrium around them. This constraint allows us to keep the same dynamics and topology as if the cores were free to rotate, but with the added freedom to explicitly compare differently oriented dressed NP-NP interactions. To calculate the NP-NP separation dependence of the free energy, we exploit the periodic boundaries of the simulation

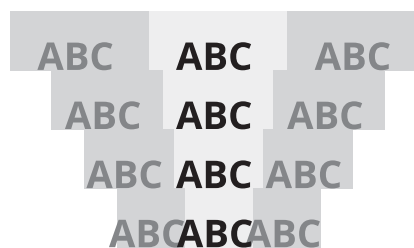


FIG. 1. Schematic representation of the periodic boundary compression method. The left side of NP "A" interacts with the right side of NP "C" across the periodic boundary. The distance between the particle centers is changed by adjusting the length of the simulation box.

cell, as illustrated by the image in Fig. 1. The direct interactions between ligand pseudo-atoms on opposite sides of the NP are very weak since their separations are of the order of the core diameter, which is an order of magnitude larger than the length scale for the interaction between the pseudo-atoms. Therefore, rather than explicitly simulating a system with two NPs in which only a small fraction of the pseudo-atoms will contribute to the direct interaction, we allow a single NP to interact with itself across a single periodic boundary. In essence, the right side of the NP will see the left side as if the ligands were attached to a different core. When we want to vary the core-core separation between the NPs, then we only need to vary the size of the simulation cell. Since the core and sulfur atoms are kept with the fixed position in this picture, varying the NP-NP distance in this manner samples separation without explicitly moving the particles or giving them any artificial velocity, thereby avoiding complications with changing temperature due to changes in the velocities of the pseudo-atoms. A similar method was used to probe the interaction between PbSe nanoparticles in Ref. 27.

Viewed as a strictly geometric construct, the method of calculation just described will yield a combination of two- and three-body contributions to the free energy. The validity of the method for the calculation of the pair potential of mean force absent three-body contributions depends crucially on the weakness of the direct interactions between ligand pseudo-atoms on opposite sides of the NP and the consequent limitation of the domains of distortion of the ligand conformations induced by interactions to the facing hemispheres of a particle and its image. When that condition is fulfilled, the method of calculation is free of three body contributions to the pair potential of mean force arising from image interactions along the line of centers of the pair. Complementing the estimate of the distant ligand-ligand interactions obtained from the potential fields we use in these calculations, we note that Schapotschnikow and Vlugt²³ report that the directly calculated three-body contribution to the free energy of three NPs is small everywhere that there is not direct overlap of the ligand distributions of the NPs, e.g., in a linear arrangement, and that Bauer *et al.*⁴⁰ find the same result. The validity of the assumption that the domains of distortion of the ligand conformations induced by interactions are restricted to the facing hemispheres of a particle, and its image can be

tested *a posteriori* by examination of the shape of the ligand distribution as a function of center-to-center particle separation. Indeed, the results displayed in Sec. III verify that assumption.

All of our simulations are performed using the Large Scale Atomic/Molecular Massively Parallel Simulator (LAMMPS) package with an NVE ensemble and a Langevin thermostat.⁵¹ To start a simulation run, we choose a random orientation for the NP and fix the simulation cell size (periodicity) so that the core-replica core separation is 100 Å and the NP will not interact with its image. The NP is thermalized at 5000 K for 0.1 ns to erase the memory of the ligand's initial straight-chain conformation. The temperature is then gradually reduced over another 0.1 ns until it reaches 300 K. The particle is allowed to equilibrate at this temperature for 5 ns. After equilibration, the simulation cell size is slowly reduced at a rate of 1 Å/ns. Once the particle has moved 1 Å, we fix the simulation cell size and let the particle equilibrate again for another 1 ns. After this equilibration, we let the particle evolve for an additional 1 ns, during which time we collect data (energies and pseudo-atom trajectories). After the data collection period, the NP-NP separation is changed and this process is repeated until the particles have reached the minimum separation of 51 Å. For the region between 75 Å and 51 Å, we sampled with a higher spatial resolution than from 100 Å to 75 Å, namely, every 0.33 Å, changing the periodicity at 0.33 Å/ns, but still equilibrating and collecting data for the same time. We repeated this procedure while varying the compression rates and equilibration times and found that allowing the system to equilibrate for substantially longer periods (~10× longer) or changing the periodicity much more slowly (~10× slower) did not substantially affect the resulting energies or pseudo-atom trajectories. Conversely, reducing the equilibration time by roughly a factor of five, or increasing the compression rate beyond 10 Å/ns, led to the energy growing over the course of the simulation, implying that the compression was driving the system out of equilibrium. By keeping the equilibration times long and the compression rates small, we ensure that the transitions between separations occur quasi-statically.

III. RESULTS FROM THE CALCULATIONS

A. The pseudo-atom model pair potential of mean force

For each configuration with a fixed NP-NP separation defined with respect to the image NP, fixed NP orientation, and fixed NP ligand coverage, the time average over the potential energies in the space of ligand conformations gives the constrained free energy of interaction for that NP-NP separation and NP orientation. Repetition of the procedure for different NP-NP separations yields the constrained potential of mean force for the fixed NP orientation; the average of the latter over NP orientations yields the unconstrained potential of mean force. This method of calculating the potential of mean force through constrained molecular dynamics is well described in the literature.^{17,24,52-57}

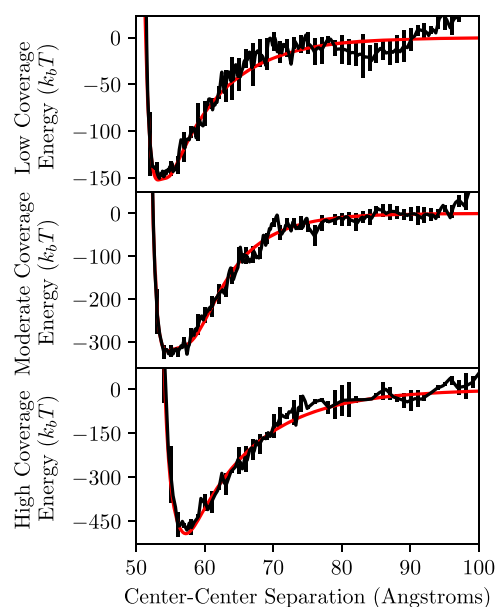


FIG. 2. Comparison of the computed pair interaction free energy (black) with the fit to Eq. (3.1). The ligand coverages are $C_{\text{Low}} = 0.32$, $C_{\text{Moderate}} = 0.64$, and $C_{\text{High}} = 0.96$.

A sample of the results of our calculations of the pseudo-atom model NP-NP potential of mean force is displayed in Fig. 2. Except for very low ligand coverage, in which

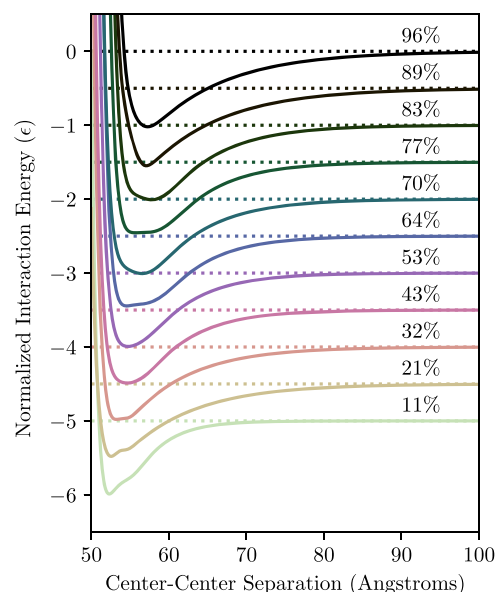


FIG. 3. The pair interaction free energies as a function of ligand coverage. The curves shown are the fits of the simulation data to Eq. (3.1). The well depths of all of the potentials have been normalized to -1 and successive potentials are shifted by 0.5 so that the shapes of the pair interaction free energies with different ligand coverages can be better compared.

case the shape of the NP-NP repulsive interaction is poorly constrained, we find that the pair potential of mean force separation dependence is well represented by the sum of an algebraic repulsive term, an exponential attractive term, and a Gaussian correction term with coverage dependent parameters

$$U(r) = \epsilon \left[\left(\frac{\sigma_R}{r} \right)^{64} - e^{-(r-r_A)/\alpha_A} + G e^{-(r-r_G)^2/(2\sigma_G^2)} \right]. \quad (3.1)$$

Equation (3.1) is found to accurately represent both the depth and the shape of the potential of mean force with variation of the ligand coverage (see Figs. 2 and 3). As shown in Fig. 4, the length scales for the repulsion (σ_R), the well minimum (r_0), and the attraction (r_A) grow linearly with the ligand coverage. The ligand coverage dependence of the scale length for the exponential attraction (α_A) displays a deviation from linearity at small ligand coverage that we attribute to the statistics of the small number of NP orientations used in the calculation. The position of the center of the Gaussian correction term, which provides a relatively small contribution to the total energy, is linear in the ligand coverage, but its amplitude and width vary somewhat with ligand coverage. The scatter in both the amplitude and the width at high coverage is likely an artefact of the fact that different NP orientations are associated with nearly identical pair potentials of mean force with small Gaussian corrections that are not determinable with great accuracy.

A very striking feature of the pair potentials of mean force displayed in Fig. 2 is their well depth, which grows linearly

with ligand coverage up to $\sim 500k_B T$ at the highest coverage. Similar well depths have been found in studies of other ligated nanoparticles.^{23,27} Qualitative support for the reality of this finding comes from experimental studies of the structure and mechanical properties of films of dressed Au nanoparticles.⁵⁸ X-ray scattering and TEM imaging surveys of dressed Au nanoparticle films have found that the diffraction pattern and real space structure are largely independent of the surface pressure in the film, consistent with nanoparticle aggregation into large rafts even at a low surface pressure, which is the expected behavior when the NP-NP attractive well depth is large compared with $k_B T$.^{59,60} And, these films have been found to be very strong with Young's moduli on the order of several GPa and consistent with the Young's modulus of a film of NPs constructed using our pair potential of mean force.⁴⁷

These calculations reveal some interesting features of the pair potential of mean force when the ligand coverage is small. First, we find that for a few NP orientations there is negligible ligand-mediated NP-NP repulsion so that the repulsive component of the interaction is then completely due to the core-core interaction. This situation is consistent with the occurrence of sintering, when nanoparticles bind together with their cores in contact. We only observe this behavior in our simulations at a very low surface coverage, well below the coverage where it has been observed experimentally. We argue that this discrepancy can be attributed to the immobility of ligands along the surface of our simulated nanoparticles.

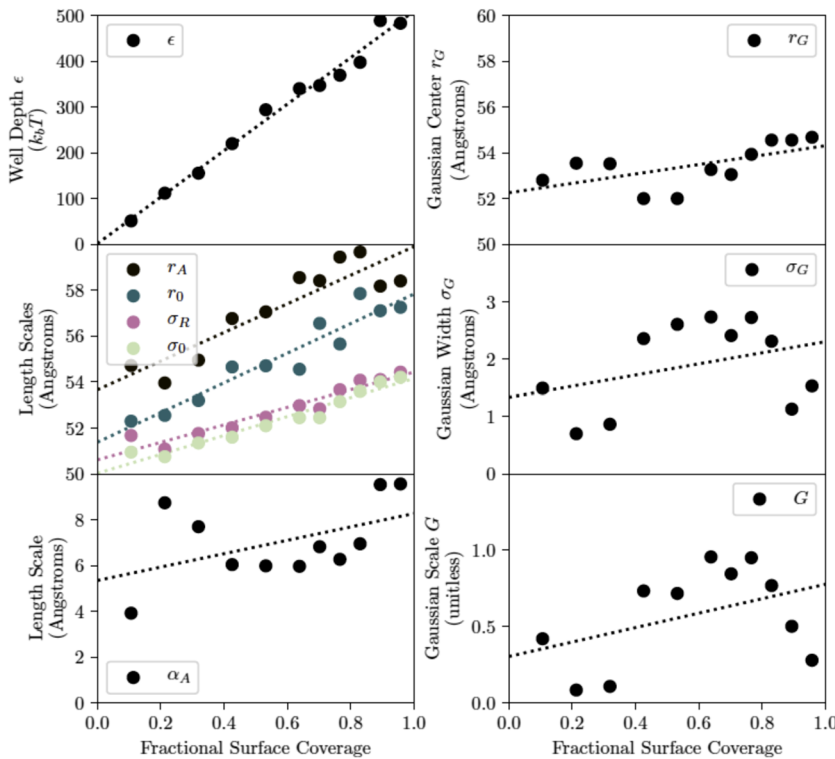


FIG. 4. The dependence of the parameters in Eq. (3.1) on ligand coverage. The minimum of the potential is at r_0 and $U(\sigma_0) = 0$.

Since a single ligand occupying the region surrounding the line of closest approach of the cores will produce a strong repulsion between the cores that arises from its bending whilst the core-core separation decreases, it will be energetically preferable for that ligand to migrate along the core surface away from the approaching core if it can. This migration will affect the distribution of core-core, core-ligand, and ligand-ligand orientations and for a specific moderate coverage will allow for more core-core interaction than does a fixed distribution of ligand coverage.

Second, at low coverage we observe that there is a large variation between the pair potentials of mean force for nanoparticles with different orientations. As described above, this variation is to be expected given the large inhomogeneity of the ligand topography in the low coverage limit. We observe that the potentials of mean force for different NP orientations become more uniform as the ligand coverage increases, and for C larger than ~ 0.43 the variations between the different orientations sensibly vanish. In experiments, the ligand coverage is restricted by the surface chemistry between the ligands and the gold^{48,61} since the surface coverage must remain in equilibrium with the concentration of ligands in the solvent surrounding the NPs. When the surface coverage is small, ligands will tend to attach to open regions on the surface, but the coverage can only remain small if the solvent is sensibly free of ligands. In the experimental preparation process, the NPs are washed several times by repeatedly replacing the solvent with one that is devoid of ligands. Although the ligand coverage can be modulated, in practice it can only be reduced to about $C = 0.7$.⁴⁶ Combining this information with the results of our calculations, we infer that in the experimentally relevant situations we can treat the dressed NPs as spherically symmetric particles.

Third, the Au surface-to-Au surface separation between dodecane thiol-ligated gold NPs in a monolayer has been measured in TEM and x-ray scattering experiments.⁶⁰ The TEM data yield Au surface-to-Au surface separations in the range 1.4 nm–1.7 nm, which is roughly the length of a single ligand molecule. The location of the minimum of the pair potential of mean force that we have calculated grows linearly with ligand coverage, from sensibly zero for nearly bare particles to 0.7 nm for fully coated particles; at comparable coverage in the simulation and experiment we find the NP-NP pair minimum to be about one third of the ligand molecule length. One source for the discrepancy between these values is the polydispersity of the gold core diameters ($\approx 15\%$) used in the experimental studies, which likely weights the larger separations in the image analysis. Since the diameter of the gold core is much larger than the ligand molecule length, the fluctuations in the measured particle-particle spacing due to that polydispersity will have a comparable scale to the spacing between monodisperse particles. We believe that a more important source for the discrepancy is deviation from pair additivity of the free energy of the NP film. As will be shown in Sec. IV, the multi-body contributions to the NP assembly free energy are significantly large; for a ligand coverage $C = 0.96$, the minimum of the effective pair potential of mean force including three- and four-particle contributions is about 10% larger than for

the isolated pair potential of mean force, which brings the separations determined from experiment and simulation into qualitative agreement.

Fourth, the experimental finding that the measured NP-NP spacing is comparable to a chain length has led to some speculation that ligands on opposite particles may “interdigitate.” We do not observe this feature in our simulation results. We find, instead, that ligands on opposite particles splay out along the mid-plane between the cores rather than mix.

How robust are these observations with respect to the substitution of a pseudo-atom representation for an all-atom representation of the ligand bound to the AuNP and of the consequent ligand capped NP-NP interactions? In the best of all possible worlds, the parameterizations of the two representations would generate predictions of the isolated capped NP and of the capped NP-NP interactions that agree both qualitatively and quantitatively. Given the uncertainties associated with the choice of functional forms used in the different representations and the uncertainties associated with the evaluation of the parameters in these functional forms, it is reasonable to expect a pseudo-atom representation to correctly predict all the qualitative features of the ligand capped NP-NP interaction with good but not perfect accuracy. As part of an investigation of the influence of water vapor on the interaction between ligand capped NPs, to be reported elsewhere, we have carried out MD simulations of the pair potential of mean force between AuNPs in a vacuum using an all-atom model of dodecane thiol ligated 5 nm diameter gold nanoparticles. As for the simulations with pseudo-atom representation of the interactions, the head groups of the thiols were fixed in place and the Au cores were treated as spheres. The intramolecular and intermolecular interactions of the ligand chains were described using the OPLS-AA force field modified to account for long alkane chains, using the parameter set developed by Siu, Pluhackova, and Bockmann.⁶² The simulation cell contained two ligated NPs, so the interaction between them was calculated directly rather than with the indirect scheme described in Sec. II. A comparison of the pseudo-atom and all-atom pair potentials of mean force for AuNPs with surface coverage, 3.6 ligands/nm², is displayed in Fig. 5. Overall, the qualitative agreement between the two potentials is very good, noting that the shapes are very similar. The two potentials differ quantitatively: the depth of the all-atom pair potential of mean force is somewhat greater, and the position of the minimum somewhat larger, than for the pseudo-atom pair potential of mean force. The values of the most relevant parameters in the fits of Eq. (3.1) to the simulation data are $\epsilon_{UA} = 275k_B T$, $\epsilon_{AA} = 370k_B T$, $\sigma_{R,UA} = 53.7 \text{ \AA}$, $\sigma_{R,AA} = 58.6 \text{ \AA}$, $r_{0,UA} = 56.2 \text{ \AA}$, and $r_{0,AA} = 61.8 \text{ \AA}$. Considering the all-atom calculations, the separation at which NP-NP repulsion rises rapidly and the shift in the position of the minimum of the potential are consistent with increased stiffness and somewhat greater extension of the all-atom representation of the ligand relative to the pseudo-atom representation of the ligand. We take the overall consistency between these calculated pair potentials of mean force as verification of the utility of the pseudo-atom representation for characterization of ligated NP properties.

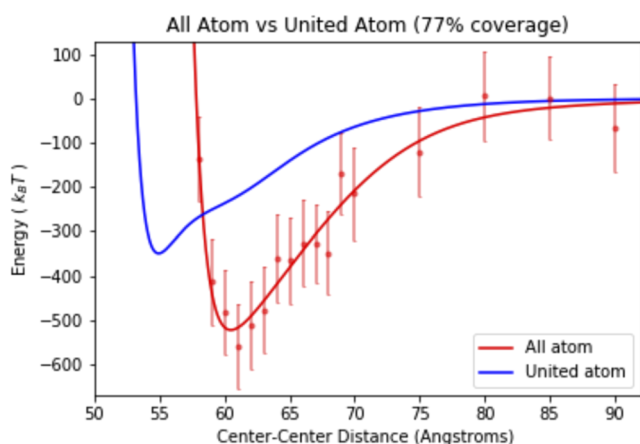


FIG. 5. Comparison of the pair potentials of mean force calculated with the united atom and all-atom representations of the ligand. The continuous curve is, in each case, the fit of Eq. (3.1) to the simulation data.

B. Pseudo-atom model ligand conformations and packing structure

Our calculations record the positions and trajectories of the pseudo-atoms of the NPs throughout the interaction. These trajectories provide information about the internal structure of the dressing ligands, specifically, the number density of pseudo-atoms throughout the ligand envelope. Since the NP pair interaction is approximately azimuthally symmetric, we define an axis linking the core-centers of the two particles. We then characterize the position of a pseudo-atom within the ligand envelope surrounding the core by its distance from the center of the core to which it is bound and the angle formed between the core-core axis and the line connecting that position to the core.

When the NP-NP pair is well separated, the individual NPs are spherically symmetric except for the small-scale angular inhomogeneity mentioned above. The NP properties

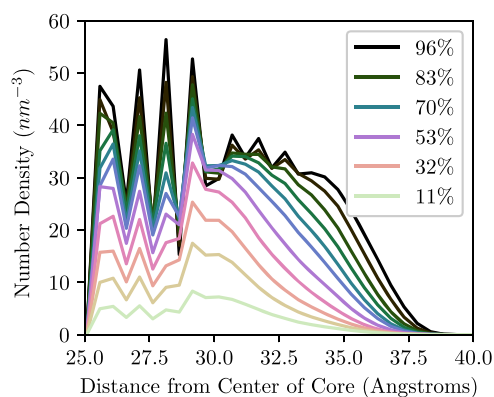


FIG. 6. Number density of pseudo-atoms as a function of distance from the NP core as a function of ligand coverage.

in this limit inform us about the equilibrium structure of the ligand envelope of an individual NP. We find that the ligand density along a radius emanating from the core, $\rho(r)$, has the same gross features for all values of C , as shown in Fig. 6.

The pseudo-atom density close to the core oscillates around a constant value up to a distance along the chain corresponding to the position of the fourth pseudo-atom and then smoothly decays to zero. This radial structure is a consequence of the fixed positions of the ligand attachments to the NP surface. Consequently, the motions of the first few pseudo-atoms of the ligand chain are restricted. The first triplet of pseudo-atoms is confined to very nearly forming a rigid triangle, and the first quadruplet has a single *cis* and two *gauche* conformations available; these nearly fixed conformations lead to the peaks in $\rho(r)$. At greater distance from the NP surface, there are substantially more conformations available to a ligand chain, including freedom to tilt away from the normal to

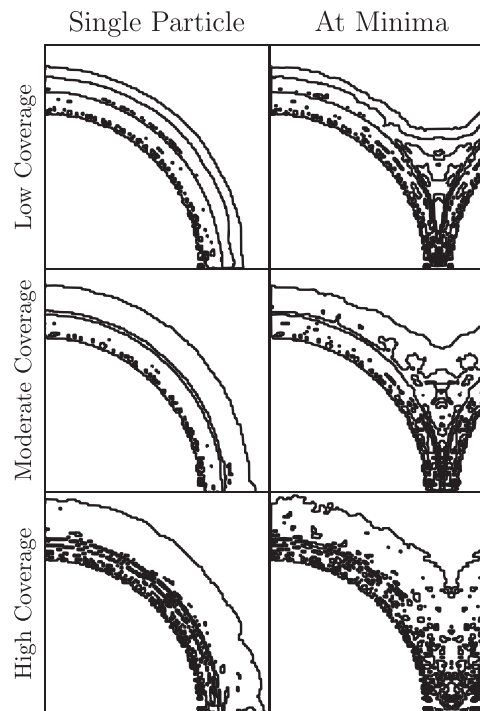


FIG. 7. Contour maps of the spatial distribution of pseudo-atoms around the NP core. The distributions are displayed in cylindrical coordinates after averaging over the azimuthal angle. The axis of the cylindrical coordinates coincides with the center-to-center line between NPs. The left column shows the ligand distribution when the core-core separation is 10 nm; the right column shows the ligand distribution at the equilibrium core-core separation. The three frames are for ligand coverages (top-to-bottom) $C = 0.32$, $C = 0.64$, and $C = 0.96$. The contour levels for $C = 0.32$ are multiples of $7.5/\text{nm}^3$ (7.5, 15, 22.5, 30, 37.5, 45, 52.5, and 60) progressively smaller from the NP surface outwards. The contour levels for $C = 0.64$ are at multiples of $15/\text{nm}^3$ (with a maximum of $120/\text{nm}^3$), progressively smaller from the NP surface outwards. The contour levels for $C = 0.96$ are multiples of $22.5/\text{nm}^3$ (with a maximum of $180/\text{nm}^3$) progressively smaller from the NP surface outwards.

the surface, noting that said tilt is restricted by the presence of neighboring ligands.

Near the NP core the density of pseudo-atoms in the ligand chains is proportional to the coverage on the surface, even down to very low coverage, indicating that the density in that region is strictly due to the changing number of chains attached. This observation implies that the ends of the chains are not bending back into the interior region, as that would increase the observed density at low coverage. Since the density-coverage proportionality holds down to low coverage, it cannot be attributed to exclusion effects from neighboring ligands alone. Instead, it can be understood as another consequence of the limited flexibility of the ligand chains. The torsion potential keeps the chain rigid on the scale of a third of the chain length. Although at the unbound end of the chain, there are many configurations very few include chain reversal. For ligand coverage greater than $C = 0.8$, the pseudo-atom density distribution has small peaks out to about the seventh position in the ligand chain, after which it decays continuously to zero, whereas for ligand coverage less than 0.8, the pseudo-atom density distribution decays continuously to zero for separations beyond the fourth position in the ligand chain.

We now consider the ligand pseudo-atom density distribution as a function of the NP-NP separation. Contour plots of three ligand density distributions in the isolated particle and in a NP-NP pair at the respective equilibrium separations are shown in Fig. 7. Figure 8 displays the radial distributions of ligand density at several angles with respect

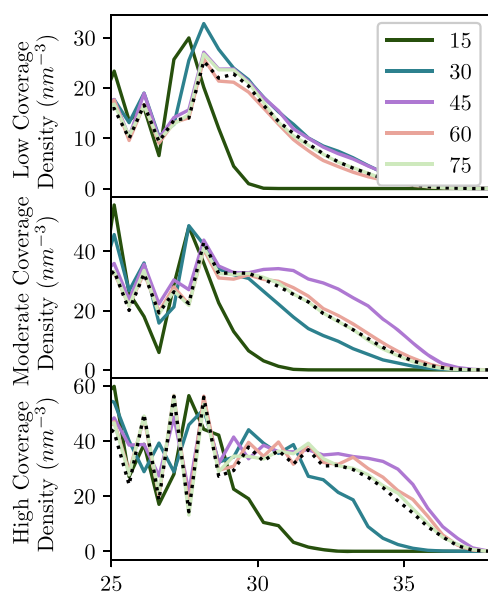


FIG. 8. Cross sections of the spatial distributions of pseudo-atoms around the Au core along lines with fixed angular separation from the line between core centers, all for the equilibrium core-core separation for the angles labelled in the inset. The single particle ligand distributions shown in Fig. 5 are here represented as the black lines. From top-to-bottom, $C = 0.32$, $C = 0.64$, and $C = 0.96$.

to the center-to-center axis. At low coverage, the NP-NP interaction generates a small region close to the center-to-center axis where the ligand density has been highly enhanced, but there is virtually no enhancement of the ligand density at angles beyond 15° from the axis. Conversely, at high coverage the pair interaction generates only a small enhancement of the ligand density along the center-to-center axis, but that enhancement extends to angles far away from the axis. As the coverage varies from low to high, there is a smooth shift between these behaviors. The fractional change in the density in the interacting region decreases gradually with increasing coverage, while the angular range over which that density is affected grows until the entire particle is involved.

IV. NON-ADDITIVITY OF THE PAIR POTENTIAL OF MEAN FORCE

Our simulation data reproduce the qualitative features of the pair potential of mean force inferred from earlier simulations,¹⁰⁻³⁷ and they extend the coverage of the parameters that influence the pair potential of mean force; the quantitative differences between the results of the several simulations arise from differences in the model NPs (e.g., core diameter and ligand coverage), and they use different parametric representations of the ligand conformations and the ligand-ligand interactions. The calculations reported in this paper clearly show that the pair potential of mean force is sensitive to the coverage of the NP by the ligands and the character of the ligand conformations, and that the distribution of ligand conformations depends on the NP-NP separation. The distribution of ligand conformations in an NP-NP pair retains statistical cylindrical symmetry, but not spherical isotropy, and the loss of the latter has been suggested to be the driver for anisotropic NP structures, such as strings of NPs.^{63,64} Of more relevance to us, the distribution of ligand conformations on each of the NPs of a pair separated by some fixed distance is expected to be further changed when other NPs are nearby, in which observation implies that the free energy of assembly of NPs will have a non-trivial multi-particle contribution augmenting the sum of pair potentials of mean force. Moreover, we expect that the magnitude of the deviation from pair additivity of the potential of mean force will depend on the ligand coverage.

For simple particles that interact with a central potential there exists a rarely exploited systematic formalism for calculation of the corrections to additivity of the pair potential of mean force. That formalism defines successive corrections to the representation of the triplet correlation function by the product of pair distribution functions^{65,66} via an expansion in powers of the system density. However, the calculation of the coefficients in the power series is too complex to be practical for the case of the typical NP-NP interaction.⁶⁷ The calculations of the three NP correction to pair additivity of the potential of mean force that have been reported utilize a direct calculation of the work required to assemble particular configurations of three NPs in a vacuum. These calculations, reported by Schapotschnikow and

Vlugt,²³ and by Bauer *et al.*,⁴⁰ provide the following relevant information:

- (1) For the dodecane thiol ligated model NPs studied by Bauer *et al.*, when 3 NPs are in an equilateral configuration with separations $r_{12} = r_{13} = r_{23}$ equal to the two-particle equilibrium separation, the three-particle correction interaction is repulsive and amounts to about 30% of the total interaction. When the triangular configuration of particles subtends an angle greater than 60° , say, with r_{12} and r_{23} fixed, or when r_{12} is increased with r_{23} and the angle between r_{12} and r_{23} fixed, the three-body correction interaction decreases. In general, for all the configurations considered, the correction to additivity of the pair potential of mean force is found to be sensibly monotonically repulsive as a function of all pair separations.
- (2) The range of the three-particle correction interaction is a fraction of a core diameter. For example, the calculations reported by Bauer *et al.* show that for an isosceles triangle arrangement of dodecane thiol ligated cores with diameter 3.7 nm, with r_{12} fixed at the equilibrium NP-NP separation determined by the pair potential of mean force ($\cong 1.33$ core diameters), the three-particle correction interaction is reduced to sensibly zero when $r_{13} = r_{23}$ are increased to 1.7 core diameters. At fixed NP-NP separation, the three-particle correction interaction is decreased when the core diameter is increased. We will make use of these observations in our treatment of the interaction free energy of a square-lattice system (see below).
- (3) As expected, the angular distribution of the deformation of the conformations of the ligands dressing a NP that approaches a pair of NPs with fixed separation depends on the deviation of the line of approach from perpendicular to the line of centers of the NP pair; the loss of symmetry of these deformations and overlap of their angular spreads contribute to the multiparticle correction interactions.
- (4) The angular dependence of the three-particle correction interaction is strong. Using results from the simulations reported by Bauer *et al.*, for the equilateral triangle configuration with all NP-NP separations equal to that determined by the isolated pair potential of mean force the three-particle correction interaction is approximately 250 kJ/mol, whereas with the same particle separations in the right triangle configuration the three-particle correction interaction is only 75 kJ/mol.
- (5) Schapotschnikow and Vlugt have reported the results of simulations of three-particle interactions between butane thiol and octane thiol capped NPs with Au core diameter 1.8 nm. If 1, 2, and 3 identify the three NPs, they calculate an effective pair potential of mean force that is defined by integration of the projection of the sum of the forces between particles 1 and 3, and 2 and 3, onto the bisector of the separation between particles 1 and 2. With the potential parameters they

used for the octane thiol capped NPs, the three-body correction to additivity of the pair potential of mean force is found to be monotonically repulsive. These calculations predict that the three-particle correction to pair additivity vanishes when the NP-NP separation exceeds the distance at which the capping ligand chains overlap.

- (6) For all configurations of the three particles with separations that permit ligand chain overlap it is found that the equilibrium NP-NP separation is increased from that determined by the isolated pair potential of mean force, and that the well depth is reduced from that determined by the isolated pair potential of mean force.

Because of the complexity and great number of degrees of freedom of the capping ligands, we expect that bringing an extra NP close to a compact cluster of NPs will generate a perturbation to the capping ligand distribution of each NP in the cluster and an extra non-trivial correction to the additivity of the pair potential of mean force beyond the three-body, four-body, . . . , corrections. All of these multi-particle corrections have, in general, complicated dependences on the geometry of the cluster. Since much of the interest in NP systems is in the properties of close packed ordered assemblies of particles, we examine a simplified representation of the role of non-additivity of the pair potential of mean force with a proxy function. Specifically, we examine the NP-NP separation dependence of a defined effective pair potential of mean force that plays the role of a “bond” potential. This proxy function includes, implicitly, the variation along one specific symmetry coordinate of all of the non-additive contributions to the free energy in the cluster; the defined proxy function depends only on the NP-NP separation. The model cluster we have considered is extracted from a periodic square lattice of NPs; it was designed to have enough NPs that more than three-body corrections to the pair potential of mean force contribute to the free energy, and a symmetry that permits straightforward definition of the effective pair potential of mean force.

The square lattices we consider were constructed in the same manner as the linear systems described above, except with two periodic boundaries instead of just one and with the x and y length scales kept identical. As before, we explicitly model just one NP but we allow that NP to interact with its images across the periodic boundaries. To vary the lattice constant of the arrangement, we slowly increase or decrease the size of the simulation box preserving the square symmetry, and we extract the NP-NP separation dependence of an effective pair potential of mean force from the total interaction free energies of the expanded/contracted configurations. By construction, the total interaction free energy includes contributions due to the interactions between the NP and its images, which will be affected by the ligand distribution perturbations generated by other images, i.e., the total interaction free energies will contain contributions from three, four, and higher particle correction interactions.

Though direct interactions between diagonal neighbors in the lattice are allowed, we expect them to only present

a minor contribution to the total interaction free energy as the calculations reported in this paper show that the pair potential of mean force of fully capped NPs at a separation of 1.4 core diameters is only of order 7% of the well depth at the equilibrium separation (see Fig. 2). Similarly, the calculations of Schapotschnikow and Vlught show that the three-particle correction to the additivity of the potential of mean force is vanishingly small when pair separation exceeds the separation for incipient ligand chain overlap. We can therefore interpret the total interaction free energy as the sum of effective pair potentials of mean force between nearest neighbors in the lattice, i.e., the “bond” pair potentials of mean force, and interpret the difference between the defined “bond” pair potential and the isolated pair potential described above as the cumulative effect of three-, four-, and higher-particle corrections.

We have calculated the total interaction free energies of square configurations of NPs with three different ligand coverages; Fig. 9 displays the defined effective pair potentials of mean force, and Fig. 10 displays the difference between the effective potentials and the corresponding isolated pair potentials of mean force for the several ligand coverages. These calculations reveal three important features of the deviation from additivity of the pair potential of mean force. First, as reported by others, the depth of the well in the effective pair potential of mean force differs from that between an isolated pair of NPs. This difference in depth is ligand coverage dependent. Second, for the ligand coverage range considered the position of the minimum in the effective pair potential of mean force is shifted to larger separation than that between an isolated pair of NPs with the same coverage. We find that the well of the effective pair potential of mean force is deeper at small coverage and shallower at high coverage than that of the pure pair potential of mean force.

We now examine how the three- and higher-particle correction interactions to the pair potential of mean force generate the observed changes in well depth and NP-NP equilibrium separation. Our definition of the effective pair potential of mean force does not reveal the partitioning of the correction interactions between the three-, four-, and higher-particle

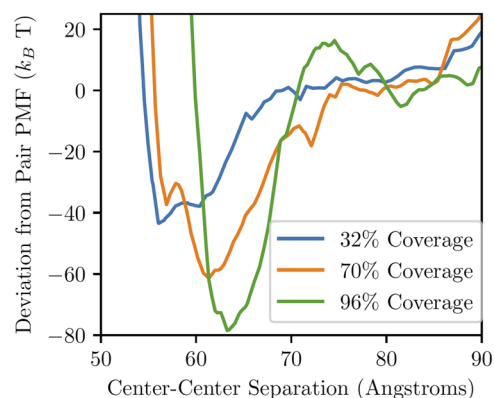


FIG. 10. Difference between the effective pair potential of mean force and the isolated pair potential of mean force. From top-to-bottom, $C = 0.32$, $C = 0.64$, and $C = 0.96$.

contributions. The calculations reported by Schapotschnikow and Vlught and by Bauer *et al.*, both show that for fully capped NPs the correction interaction induced by the third-particle perturbation of a pair of NPs is monotonically repulsive. The magnitudes of the well depths displayed in Fig. 9, combined with the magnitudes of the three-particle correction interaction computed by Schapotschnikow and Vlught, and by Bauer *et al.*, imply that the four- and higher-particle correction interaction is comparable in magnitude to the three-particle correction interaction but of opposite sign, i.e., attractive. We argue that the importance of the many particle corrections to additivity of the potential of mean force is visualized in dramatic changes in the ligand distribution on the surface of the Au core. We show in Fig. 11 the ligand distribution on one AuNP in the square assembly when the AuNPs are far apart (right column, center-to-center separation 8 nm) and close together (left column, center-to-center separation 5.3 nm). The dramatic transition from a spherical distribution to a near square distribution with greatly enhanced density of ligands at the corners is apparent for all three coverages (1.5 ligands/nm², 3.0 ligands/nm², and 4.5 ligands/nm²). We

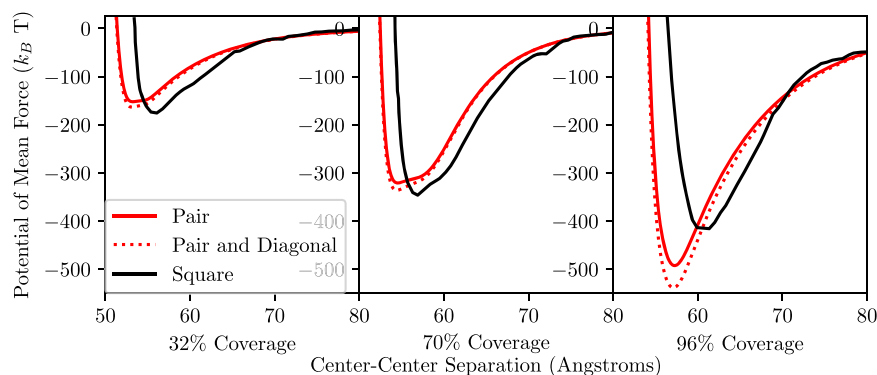


FIG. 9. Pair free energy function for an isolated NP pair (red) and inferred from the free energy of four NPs in a square (black). From top-to-bottom, $C = 0.32$, $C = 0.64$, and $C = 0.96$. The dotted red curve shows the effective pair free energy function constructed from pair interactions including the interaction along the diagonal of the square.

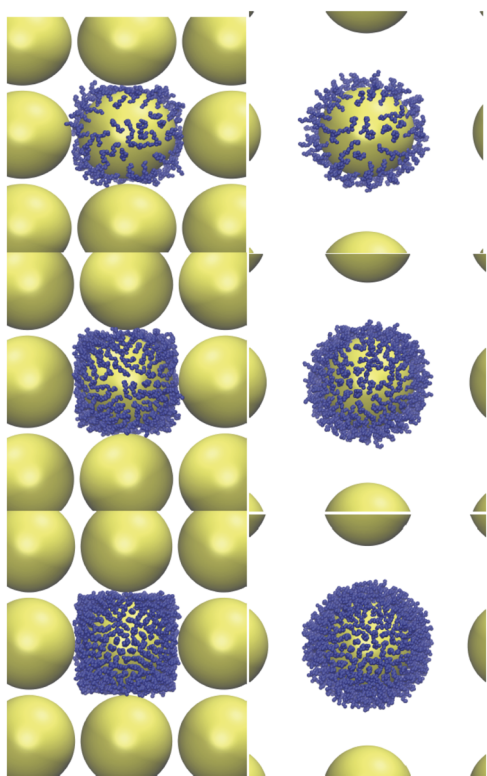


FIG. 11. Ligand distributions on a AuNP in a square array of NPs: Right column, center-to-center separation 8 nm, left column, center-to-center separation 5.3 nm, top row 1.5 ligands/nm², middle row 3.0 ligands/nm², and bottom row 4.5 ligands/nm². The ligand distributions of the NPs that neighbor the one displayed are not displayed.

conclude that it is plausible that contributions to the effective pair potential of mean force from changes in the ligand distributions induced by proximity to more particles, e.g., fifth and sixth neighbors in a two-dimensional array, may be significant.

V. DISCUSSION

In summary, our simulations of the properties of a pseudo-atom model of a dodecane thiol-ligated gold core nanoparticle in a vacuum predict that the pseudo-atom density distribution in the interior region of the ligand envelope is structured with a scale length of the pseudo-atom-pseudo-atom separation and that the outer region of the envelope has a pseudo-atom density profile that smoothly decays to zero. The NP-NP interaction in a vacuum is strongly dependent on the ligand coverage, and therefore on the density and distribution of pseudo-atoms in the envelope. In turn, the distribution of pseudo-atoms in the ligand envelope changes as the NP-NP separation changes. We have developed a simple functional form for the pair potential of mean force; this functional form has length scales characteristic of short-range repulsion and the well location, and a well depth, all of which

scale linearly with the surface coverage; the well depth which reaches up to $\sim 500k_B T$ at the highest coverage. At the minimum of the pair potential of mean force between two NPs, when the ligand coverage is low, there is localized enhancement in the density of pseudo-atoms between the particles; when the ligand coverage is high, the pseudo-atom density change is spread around the entire nanoparticle. The curvature at the minimum of the pair potential of mean force is consistent with the measured Young's modulus of a monolayer of dodecane thiol-ligated gold NPs.⁴⁶ Because the internal structures associated with the ligand chains are dependent on the ligand coverage and on the NP-NP separation, there are important multi-particle contributions to the effective pair potential of mean force. Our calculations imply that the three- and four-particle correction interactions to the additivity of the pair potential of mean force are of comparable magnitude but opposite sign and that correction interaction contributions from yet larger numbers of particles need to be investigated.

Several phenomenological models have been proposed to describe the interactions between capped nanoparticles. In particular, the Optimum Packing Model (OPM)⁶⁸ and the Overlapping Cone Model (OCM)²³ have been widely used to suggest equilibrium separations between nanoparticles. These models set the equilibrium separation as that where the volume occupied by some ligands in the system matches the free volume available for these ligands. The OPM compares the volume occupied by a single fully extended ligand with the cone formed by the center of the core, the area of the binding site, and the midplane between the nanoparticles. The OCM compares the volume of the cone formed by the center of the core, the midplane between the nanoparticles, and the edge of the ligand envelope with the volume of the ligands which are bound within that cone. Both models are intuitively easy to grasp and predict equilibrium separations which are in good agreement with experimental data, but the microscopic picture proposed does not agree with the results of our simulations. In essence, the OCM and the OPM assume that within the overlapping region the density of particles grows until the region is fully packed. This increase in the density fully accounts for the lost free volume around the nanoparticle, so the density does not increase outside the cone region. But our simulations contradict this feature of the models; they show that at moderate to high ligand coverages the enhanced-density regions extend well beyond the overlapping cone region.

ACKNOWLEDGMENTS

This research was primarily supported by the University of Chicago Materials Research Science and Engineering Center, funded by the National Science Foundation (Grant No. DMR-1420709), and partially supported by a Senior Mentor Grant from the Camille and Henry Dreyfus Foundation (Grant No. SI-14-014). B.L. acknowledges the support from Chem. Mat-CARS (Grant No. NSF/CHE-1346572). We thank Kevin Slater and Michael Martinez for the calculations displayed in Fig. 5.

APPENDIX: PSEUDO-ATOM POTENTIAL PARAMETERS

TABLE I. Interactions used in the model.

Core-core	$U_{cc}(r) = -\frac{A_{cc}}{12} \left[\frac{D^2}{r^2 - D^2} + \frac{D^2}{r^2} + 2 \ln \left(\frac{r^2 - D^2}{r^2} \right) \right]$ $+ \frac{A_{cc}}{75600} \frac{\sigma_c^8}{r} \left[\frac{2r^2 - 14DR + 27D^2}{(r-D)^7} + \frac{2r^2 + 14DR + 27D^2}{(r+D)^7} - \frac{4r^2 - 30D^2}{r^7} \right]$
Core-pseudoatom	$U_{cp} = \frac{16D^3 \sigma_{cp}^3 A_{cp}}{9(D^2 - 4r^2)^3} \left[1 - \frac{64\sigma_{cp}^6 (5D^6 + 180D^4 r^2 + 1008D^2 r^4 + 960r^6)}{15(D-2r)^6 (D+2r)^6} \right]$
Unbonded pseudoatom-pseudoatom	$U_{pp} = 4\epsilon \left[\frac{\sigma_p^{12}}{r^{12}} - \frac{\sigma_p^6}{r^6} \right]$
2-pseudoatom bond	$U_B = K_B (r - r_B)^2$
3-pseudoatom angle	$U_A = K_A (\theta - \theta_B)^2$
4-pseudoatom torsion	$U_T = A_0 + A_1 \cos \theta + A_2 \cos^2 \theta + A_3 \cos^3 \theta$

TABLE II. Parameters for interactions in the model.

Core-core	D = 50 Å $\sigma_c = 2.934$ Å
Core-pseudoatom	Au-Au $A_{cc} = 45.0$ kcal mol ⁻¹ D = 50 Å $\sigma_{cp} = 3.47$ Å
	Au-S $A_{cp} = 0$
2-pseudoatom	Au-CH ₂ $A_{cc} = 24.6$ kcal mol ⁻¹
	Au-CH ₃ $A_{cc} = 41.6$ kcal mol ⁻¹ $\sigma_{cp} = 3.47$ Å
	S-S $\epsilon = 0.0934$ kcal mol ⁻¹
	S-CH ₂ $\epsilon = 0.0934$ kcal mol ⁻¹
	S-CH ₃ $\epsilon = 0.1455$ kcal mol ⁻¹
2-pseudoatom bond	CH ₂ -CH ₂ $\epsilon = 0.0934$ kcal mol ⁻¹
	CH ₂ -CH ₃ $\epsilon = 0.1455$ kcal mol ⁻¹
	CH ₃ -CH ₃ $\epsilon = 0.2264$ kcal mol ⁻¹
2-pseudoatom bond	$K_B = 600$ kcal mol ⁻¹ Å ⁻² $r_B = 1.53$ Å
3-pseudoatom angle	$K_A = 60$ kcal mol ⁻¹ deg ⁻² $\theta_A = 109.5^\circ$
4-pseudoatom torsion	$A_0 = 1.553$ kcal mol ⁻¹ $A_1 = 4.06$ kcal mol ⁻¹ $A_2 = 0.867$ kcal mol ⁻¹ $A_3 = -6.48$ kcal mol ⁻¹

REFERENCES

- A. N. Shipway, E. Katz, and I. Willner, *Chem. Phys. Chem.* **1**, 18 (2000).
- Z. Nie, A. Petukhova, and E. Kumacheva, *Nat. Nanotechnol.* **5**, 15 (2010).
- A. Desireddy, C. P. Joshi, M. Sestak, S. Little, S. Kumar, N. J. Podraza, S. Marsillac, R. W. Collins, and T. P. Bigioni, *Thin Solid Films* **519**, 6077 (2011).
- P. V. Kamat, *J. Phys. Chem. B* **106**, 7729 (2002).
- X. Sun, Y. Huang, and D. E. Nikles, *Int. J. Nanotechnol.* **1**, 328 (2004).
- W. Seth Coe, W.-K. Woo, M. Bawendi, and V. Bulovic, *Nature* **420**, 800 (2002).
- J. Satija, R. Bharadwaj, V. V. R. Sai, and S. Mukherji, *Nanotechnol., Sci. Appl.* **2010**(3), 171.
- J. N. Anker, W. P. Hall, O. Lyandres, N. C. Shah, J. Zhao, and R. P. Van Duyne, *Nat. Mater.* **7**, 442 (2008).
- Y. Won Jong, Y. Cheng, Z. Gang, L. Hua Min, P. Young Jun, and K. Jong Min, *J. Korean Phys. Soc.* **56**, 1488 (2010).
- W. D. Luedtke and U. Landman, *J. Phys. Chem.* **100**, 13323 (1996).
- A.-C. Yang and C.-I. Weng, *J. Phys. Chem. C* **114**, 8697 (2010).
- A.-C. Yang, C.-I. Weng, and T.-C. Chen, *J. Chem. Phys.* **135**, 034101 (2011).
- J. M. D. Lane and G. S. Grest, *Phys. Rev. Lett.* **104**, 235501 (2010).
- B. L. Peters, J. M. D. Lane, A. E. Ismail, and G. S. Grest, *Langmuir* **28**, 17443 (2012).
- J. M. D. Lane and G. S. Grest, *Nanoscale* **6**, 5132 (2014).
- D. S. Bolinteanu, J. M. D. Lane, and G. S. Grest, *Langmuir* **30**, 11075 (2014).
- P. K. Ghorai and S. C. Glotzer, *J. Phys. Chem. C* **111**, 15857 (2007).
- W. D. Luedtke and U. Landman, *J. Phys. Chem. B* **102**, 6566 (1998).
- K. A. Tay and F. Bresme, *J. Am. Chem. Soc.* **128**, 14166 (2006).
- M. Lal, M. Plummer, N. J. Richmond, and W. Smith, *J. Phys. Chem. B* **108**, 6052 (2004).
- R. Pool, P. Schapotschnikow, and T. J. H. Vlught, *J. Phys. Chem. C* **111**, 10201 (2007).
- N. Patel and S. A. Egorov, *J. Chem. Phys.* **126**, 054706 (2007).
- P. Schapotschnikow and T. J. H. Vlught, *J. Chem. Phys.* **131**, 124705 (2009).
- P. Schapotschnikow, R. Pool, and T. J. H. Vlught, *Nano Lett.* **8**, 2930 (2008).
- A. P. Kaushik and P. Clancy, *J. Comput. Chem.* **34**, 523 (2013).
- A. Widmer-Cooper and P. Geissler, *Nano Lett.* **14**, 57 (2014).
- A. P. Kaushik and P. Clancy, *J. Chem. Phys.* **136**, 114702 (2012).
- K. M. Salerno, D. S. Bolinteanu, J. M. D. Lane, and G. S. Grest, *Phys. Rev. E* **91**, 062403 (2015).
- G. Munao, A. Correa, A. Pizzirusso, and G. Milano, *Eur. Phys. J. E* **41**, 38 (2018).
- F. LoVerso, L. Yelash, S. A. Egorov, and K. Binder, *Soft Matter* **8**, 4185 (2012).
- F. LoVerso, S. A. Egorov, and K. Binder, *Macromolecules* **45**, 8892 (2012).
- S. Hajiw, J. Schmitt, M. Imperor-Clerc, and B. Pansu, *Soft Matter* **11**, 3920 (2015).
- L. Baran and S. Sokolowski, *Appl. Surf. Sci.* **396**, 1343 (2017).
- H. O. S. Yadav and C. Chakravarty, *J. Chem. Phys.* **146**, 174902 (2017).
- T.-Y. Tang and G. Arya, *Macromolecules* **50**, 1167 (2017).
- L. Baran and S. Sokolowski, *J. Chem. Phys.* **147**, 044903 (2017).
- X. Liu, P. Lu, and H. Zhai, *J. Appl. Phys.* **123**, 045101 (2018).
- B. J. Henz, P. W. Chung, J. W. Andzelm, T. L. Chantawansri, J. L. Lenhart, and F. L. Beyler, *Langmuir* **27**, 7836 (2011).

- ³⁹J. M. D. Lane, A. E. Ismail, M. Chandross, C. D. Lorenz, and G. S. Grest, *Phys. Rev. E* **79**, 050501 (2009).
- ⁴⁰G. Bauer, N. Gribova, A. Lange, C. Holm, and J. Gross, *Mol. Phys.* **115**, 1031 (2017).
- ⁴¹Y. Wang, H. Chan, B. Narayanan, S. P. McBride, S. K. R. S. Sankaranarayanan, X.-M. Lin, and H. M. Jaeger, *ACS Nano* **11**, 8026 (2017).
- ⁴²A. S. Barnard, N. P. Young, A. I. Kirkland, M. A. Van Huis, and H. Xu, *ACS Nano* **3**, 1431 (2009).
- ⁴³K. Koga and K. Sugawara, *Surf. Sci.* **529**, 23 (2003).
- ⁴⁴Y. Wang, S. Teitel, and C. Dellago, *Chem. Phys. Lett.* **394**, 257 (2004).
- ⁴⁵R. Everaers and M. R. Ejtehadi, *Phys. Rev. E* **67**, 041710 (2003).
- ⁴⁶W. Paul, D. Y. Yoon, and G. D. Smith, *J. Chem. Phys.* **103**, 1702 (1995).
- ⁴⁷Z. Jiang, J. He, S. A. Deshmukh, P. Kanjanaboos, G. Kamath, Y. Wang, S. K. Sankaranarayanan, J. Wang, H. M. Jaeger, and X. M. Lin, *Nat. Mater.* **14**, 912 (2015).
- ⁴⁸L. Strong and G. M. Whitesides, *Langmuir* **4**, 546 (1988).
- ⁴⁹M. J. Hostetler, J. E. Wingate, C.-J. Zhong, J. E. Harris, R. W. Vachet, M. R. Clark, J. D. Londono, S. J. Green, J. J. Stokes, G. D. Wignall, G. L. Glish, M. D. Porter, N. D. Evans, and R. W. Murray, *Langmuir* **14**, 17 (1998).
- ⁵⁰G. H. Woehrle, L. O. Brown, and J. E. Hutchison, *J. Am. Chem. Soc.* **127**, 2172 (2005).
- ⁵¹S. Plimpton, *J. Comput. Phys.* **117**, 1 (1995).
- ⁵²J.-M. Depaepe, J.-P. Ryckaert, E. Paci, and G. Ciccotti, *Mol. Phys.* **79**, 515 (1993).
- ⁵³P. Schapotschnikow and T. J. H. Vlugt, *J. Phys. Chem. C* **114**, 2531 (2010).
- ⁵⁴W. K. Den Otter and W. J. Briels, *J. Chem. Phys.* **109**, 4139 (1998).
- ⁵⁵M. Sprik and G. Ciccotti, *J. Chem. Phys.* **109**, 7737 (1998).
- ⁵⁶G. Ciccotti, R. Kapral, and E. Vanden-Eijnden, *ChemPhysChem* **6**, 1809 (2005).
- ⁵⁷D. Trzesniak, A.-P. E. Kunz, and W. F. van Gunsteren, *Chem. Phys. Chem.* **8**, 162 (2007).
- ⁵⁸J. He, P. Kanjanaboos, N. L. Frazer, A. Weis, X. M. Lin, and H. M. Jaeger, *Small* **6**, 1449 (2010).
- ⁵⁹D. G. Schultz, X.-M. Lin, D. Li, J. Gebhardt, M. Meron, P. J. Viccaro, and B. Lin, *J. Phys. Chem. B* **110**, 24522 (2006).
- ⁶⁰S. D. Griesemer, S. S. You, P. Kanjanaboos, M. Calabro, H. M. Jaeger, S. A. Rice, and B. Lin, *Soft Matter* **13**, 3125 (2017).
- ⁶¹D. S. Karpovich and G. J. Blanchard, *Langmuir* **10**, 3315 (1994).
- ⁶²S. W. Siu, K. Pluhackova, and R. A. Bockmann, *J. Chem. Theory Comput.* **8**, 1459–1470 (2012).
- ⁶³P. Ackora, H. Liu, S. K. Kumar, J. Moll, Y. Li, B. C. Benicewicz, L. S. Schadler, D. Acehan, A. Z. Panagiotopoulos, V. Prymatisyn, V. Ganesan, J. Ilavsky, P. Thiyagarajan, R. H. Colby, and J. F. Douglas, *Nat. Mater.* **8**, 354 (2009).
- ⁶⁴D. Bedrov, G. D. Smith, and L. Li, *Langmuir* **21**, 5251 (2005).
- ⁶⁵E. Meeron, *J. Chem. Phys.* **27**, 1238 (1957).
- ⁶⁶E. E. Salpeter, *Ann. Phys.* **5**, 183 (1958).
- ⁶⁷A. D. J. Haymet, S. A. Rice, and W. G. Madden, *J. Chem. Phys.* **74**, 3033 (1981).
- ⁶⁸U. Landman and W. D. Luedtke, *Faraday Discuss.* **125**, 1 (2004).